doi:10.1016/j.jmb.2007.06.060 J. Mol. Biol. (2007) 372, 470–484

JMB

Available online at www.sciencedirect.com

ScienceDirect

ELSEVIER

Characterisation of Amyloid Fibril Formation by Small Heat-shock Chaperone Proteins Human αA-, αB- and R120G αB-Crystallins

Sarah Meehan[1], Tuomas P. J. Knowles[2], Andrew J. Baldwin[1] Jeffrey F. Smith[2], Adam M. Squires[3], Phillip Clements[4] Teresa M. Treweek[5], Heath Ecroyd[4], Gian Gaetano Tartaglia[1] Michele Vendruscolo[1], Cait E. MacPhee[6], Christopher M. Dobson[1]* and John A. Carver[4]*

[1]*Department of Chemistry University of Cambridge Lensfield Road, Cambridge CB2 1EW, United Kingdom*

[2]*Nanoscience Centre University of Cambridge Cambridge CB3 OFF United Kingdom*

[3]*School of Chemistry University of Reading PO BOX 224, Whiteknights Reading, RG6 6AD United Kingdom*

[4]*School of Chemistry and Physics University of Adelaide, Adelaide South Australia 5005, Australia*

[5]*Graduate School of Medicine University of Wollongong Wollongong, New South Wales 2522, Australia*

[6]*School of Physics, James Clerk Maxwell Building, The King's Buildings, University of Edinburgh, Mayfield Road Edinburgh, EH9 3JZ United Kingdom*

**Corresponding authors*

αB-Crystallin is a ubiquitous small heat-shock protein (sHsp) renowned for its chaperone ability to prevent target protein aggregation. It is stress-inducible and its up-regulation is associated with a number of disorders, including those linked to the deposition of misfolded proteins, such as Alzheimer's and Parkinson's diseases. We have characterised the formation of amyloid fibrils by human αB-crystallin in detail, and also that of αA-crystallin and the disease-related mutant R120G αB-crystallin. We find that the last 12 amino acid residues of the C-terminal region of αB-crystallin are predicted from their physico-chemical properties to have a very low propensity to aggregate. ^{1}H NMR spectroscopy reveals that this hydrophilic C-terminal region is flexible both in its solution state and in amyloid fibrils, where it protrudes from the fibrillar core. We demonstrate, in addition, that the equilibrium between different protofilament assemblies can be manipulated and controlled *in vitro* to select for particular αB-crystallin amyloid morphologies. Overall, this study suggests that there could be a fine balance *in vivo* between the native functional sHsp state and the formation of amyloid fibrils.

Keywords: amyloid; fibrils; αB-crystallin; αA-crystallin; small heat-shock proteins

Introduction

Polypeptide chains have a propensity to self-assemble into β-sheet structures known as amyloid fibrils.[1] These species were initially investigated because of their connection with a wide range of dis-

Abbreviations used: DRM, desmin-related myopathy; sHsp, small heat shock protein; TEM, transmission electron microscopy; AFM, atomic force microscopy; ThT, Thioflavin T; CR, Congo red; GdnHCl, guanidine hydrochloride; TFE, trifluoroethanol.

E-mail addresses of the corresponding authors: cmd44@cam.ac.uk; john.carver@adelaide.edu.au

orders,[2,3] including, Alzheimer's, Creutzfeld–Jakob disease, and type II diabetes. More recently, there has also been interest in these highly ordered[4] protein structures in their own right and as potential candidates for the generation of novel bionanomaterials.[5] Amyloid fibrils are threadlike structures, typically unbranched, and a few nanometres in diameter with polydispersed lengths of the order of micrometres.[6] They all share a common core structure,[7] irrespective of the nature of their precursor proteins, characterised by a cross-β X-ray fibre diffraction pattern with meridional reflections of 4.7 Å and equatorial reflections of ~8-11 Å, corresponding to the distance between β-strands and the separation between β-sheets, respectively.[7] The β-strands, lying perpendicular to the fibril axis, align and assemble into extended β-sheets which stack to form protofilaments running parallel to the fibril axis.[7] Different types of fibrils comprise variable numbers of protofilaments and can vary substantially in the supramolecular assembly of these substructures. Intrinsic factors such as primary sequence, length of the constituent polypeptide chain, and extrinsic factors such as solvent conditions, and time of incubation all influence the interactions between protofilaments and the resultant morphology of the fibril.[8–10]

A particularly interesting set of proteins that has been found to convert readily into amyloid fibrils *in vitro* is that of the crystallins.[11–13] These proteins are found in eye lenses as α-, and the related β- and γ-crystallins. They are in fact laid down in the foetus and the same molecules persist throughout life in an individual,[14] and the gradual loss of lens transparency can give rise to the development of cataract.[2] Indeed, the conversion of crystallin proteins into amyloid fibrils *in vivo* has been found to be associated with certain forms of cataract.[11,15] For example, amyloid deposition by a mutant γ-crystallin appears to be the cause of an inherited murine cataract in which intra-nuclear filamentous inclusions were identified that stained the amyloid-detecting dye Congo red.[11] The major lens protein is α-crystallin, which is also a small heat-shock molecular chaperone; nevertheless, this protein converts *in vitro* into amyloid fibrils under slightly destabilising conditions.[12] α-Crystallin is a mixture of two subunits, αA- and αB-crystallin, in a ratio of ~3:1 in the eye lens, which share approximately 60% sequence identity.[16] Both subunits are present at very high concentrations in mammalian lenses where they are thought to play an important structural and chaperone role in maintaining transparency.[2,17,18]

αB-Crystallin is also located in many parts of the body as well as in the eye lens including the retina, heart, skeletal muscle, skin, brain, spinal cord, kidneys, and lungs, whereas αA-crystallin is present to a much lesser extent, for example in the spleen and thymus.[17] The amyloid fibril-forming propensity of the individual human αA- and αB-crystallin proteins has not yet, however, been reported. Here, we describe investigations of the conversion into amyloid fibrils of human αB-crystallin, and where appropriate we also investigate the amyloid propensity of αA-crystallin for comparative purposes. Further, we characterise amyloid fibril formation by the disease-related mutant R120G αB-crystallin. This single point mutation is genetically linked to cataract[19] and to the neuromuscular disorder desmin-related myopathy (DRM).[20–22] The formation of amyloid oligomers by R120G αB-crystallin has been implicated as an important pathogenic process in DRM,[23] although fibril formation by this protein has not yet been observed and characterised.

Human αB-crystallin has 175 amino acids.[16] The sequence has an amphiphilic character[17] with a hydrophobic N-terminal and central "α-crystallin" domain,[24] and a hydrophilic C-terminal extension. The three-dimensional crystal structure has not yet been determined, although predictions based on crystal structures available for non-mammalian small heat-shock proteins (sHsps) suggest the central α-crystallin domain adopts a β-sandwich structure.[25,26] In its native state, αB-crystallin self-associates into heterogeneous multimers[27] and solution NMR studies of these complexes reveal well resolved resonances arising from the highly flexible, solvent exposed C-terminal extension that corresponds to the last 12 amino acid residues.[28] It is thought that this C-terminal extension may play a role in maintaining native subunit interactions.[29]

We describe here the use of solution state ^{1}H NMR spectroscopy to investigate how the αB-crystallin polypeptide chain is organised when the protein is incorporated into an amyloid fibril. In particular, the nature of the regions protruding from the main cross-β-amyloid core is identified. We show that the arrangement of αB-crystallin into amyloid fibrils determined experimentally correlates with theoretical predictions of the aggregation propensity of this region of the sequence based on the physicochemical properties of each residue in a given environment. We demonstrate in addition that the position of equilibrium between different protofilament assemblies can be manipulated and controlled by adjusting the pH to select for particular αB-crystallin amyloid morphologies. In these investigations, the protofilament substructure of the fibrils has been analysed and defined by atomic force microscopy (AFM) imaging and statistical analysis. As well as characterising amyloid fibril formation by the ubiquitous human sHsp αB-crystallin in detail, we compare the behaviour of this protein with αA-crystallin and R120G αB-crystallin.

Results

Formation and characterisation of amyloid fibril formation by human recombinant αA-, αB-crystallin, and R120G αB-crystallin at pH 7.4

Human recombinant αB-crystallin was subjected to conditions previously found to be effective for inducing amyloid fibril formation by bovine α-crystallin;[12] αB-crystallin was dissolved at a protein concentration of 1 mg/ml in the presence of 1 M

guanidine hydrochloride (GdnHCl) (pH 7.4) and incubated at 60 °C for 2 h. Transmission electron microscopy (TEM) studies reveal that the protein readily assembles under these conditions into fibrils that are 2–10 μm in length (Figure 1(a)). In its native state, wild-type human recombinant αB-crystallin also self-associates into roughly spherical aggregates ranging from 8 nm to 18 nm in diameter.[30] After amyloid fibril assembly, the presence of native-like spherical aggregates was observed to be rare and is estimated to represent <1% of the observable protein material on the TEM sample grid. Ultracentrifugation of αB-crystallin fibril solutions results in the fibrillar material being pelleted under conditions where the native protein remains in solution and shows that under these conditions conversion of the native protein into the fibrillar state was >95% complete. Likewise, αA- and R120G αB-crystallin were also found to form amyloid fibrils at pH 7.4, with similar morphology and length to fibrils formed by αB-crystallin under the same conditions (Figure 1(a)–(c)). αB-Crystallin was also found to form similar fibrils under different conditions at neutral pH; e.g. the presence of 10% (v/v) trifluoroethanol (TFE) at pH 7.4 induces fibril formation within 30 min at 60 °C, as observed by TEM (Figure 1(d)).

Congo red (CR) and Thioflavin T (ThT) binding assays are traditionally regarded as diagnostic of amyloid-like structure,[31–33] although not without exception.[34] Indeed, fibril formation by αB-crystallin is not accompanied by a positive interaction with ThT (Figure 2(a)), an observation that has been reported for a number of other amyloid fibril systems.[35] αB-Crystallin does, however, bind CR in its fibrillar conformation (Figure 2(b)), but interestingly it does so also in its aggregated native state. This result is consistent with the observation that the crystallin proteins demonstrate apple-green birefringence with CR *in situ* in the eye lens, a property that has been attributed to their adoption of an extended β-sheet structure in the lens.[36]

X-ray fibre diffraction studies demonstrate that αB-crystallin fibrils exhibit a cross-β pattern (Figure 2(c) and (d)). No differences in the positions of the reflections were identified on comparing the X-ray patterns obtained for wild-type αB- and R120G αB-crystallin fibrils; in each case a meridional reflection at 4.7 Å, and equatorial reflections at 10.0 Å, and 23.0 Å were observed (Figure 2(c) and (d)). The kinetics of amyloid assembly were examined by measuring changes in turbidity of αB-crystallin solutions as fibril formation occurred, and indicated that the kinetics of this process follow a sigmoidal form, with a lag phase of 22(±1) min (Figure 2(e)). By comparison, the lag phase for R120G αB-crystallin aggregation is 28(±2) min, and the apparent rate constant for the growth phase of fibril formation is 60% that of the wild-type protein (Figure 2(e)). The slightly slower rate of aggregation measured for the mutant protein may imply that early aggregates, on pathway to forming full-length amyloid fibrils, persist for longer than in the case of the wild-type protein. It has been suggested previously that early amyloid aggregates are generally toxic *in vivo*,[37,38] and indeed such toxicity has been implicated in the disease-associated role of the R120G mutation;[22,23] the observation described here, therefore, could be consistent with the suggestion that the R120G mutation in αB-crystallin leads to an enhanced population of amyloid oligomers *in vivo* by this protein, resulting in the pathogenic processes associated with DRM.[22,23]

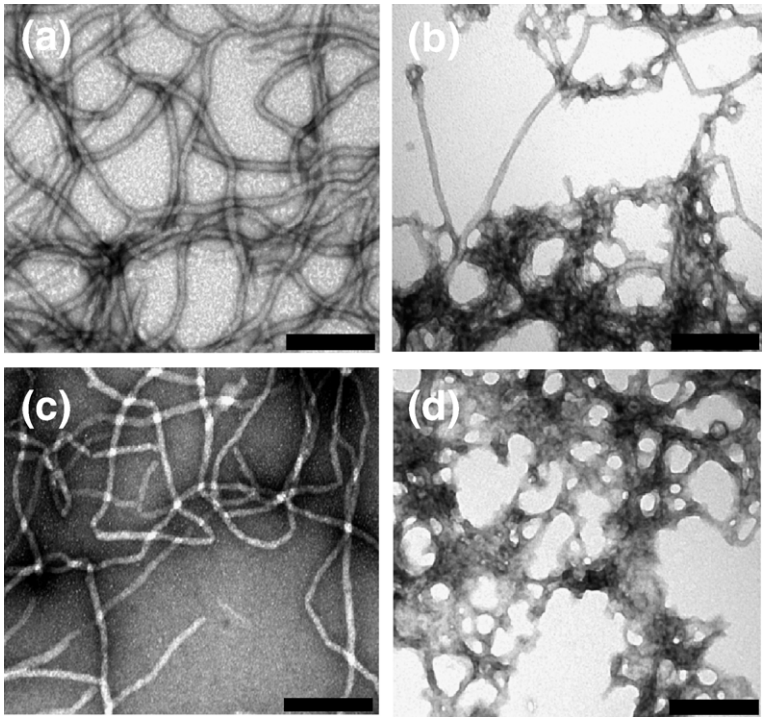

Figure 1. Fibril formation by αA-, αB-, and R120G αB-crystallins at pH 7.4. TEM images of fibrils formed with GdnHCl: (a) αB-crystallin, (b) αA-crystallin, (c), R120G αB-crystallin. (d) αB-crystallin fibrils formed with TFE. The scale bar represents 200 nm.

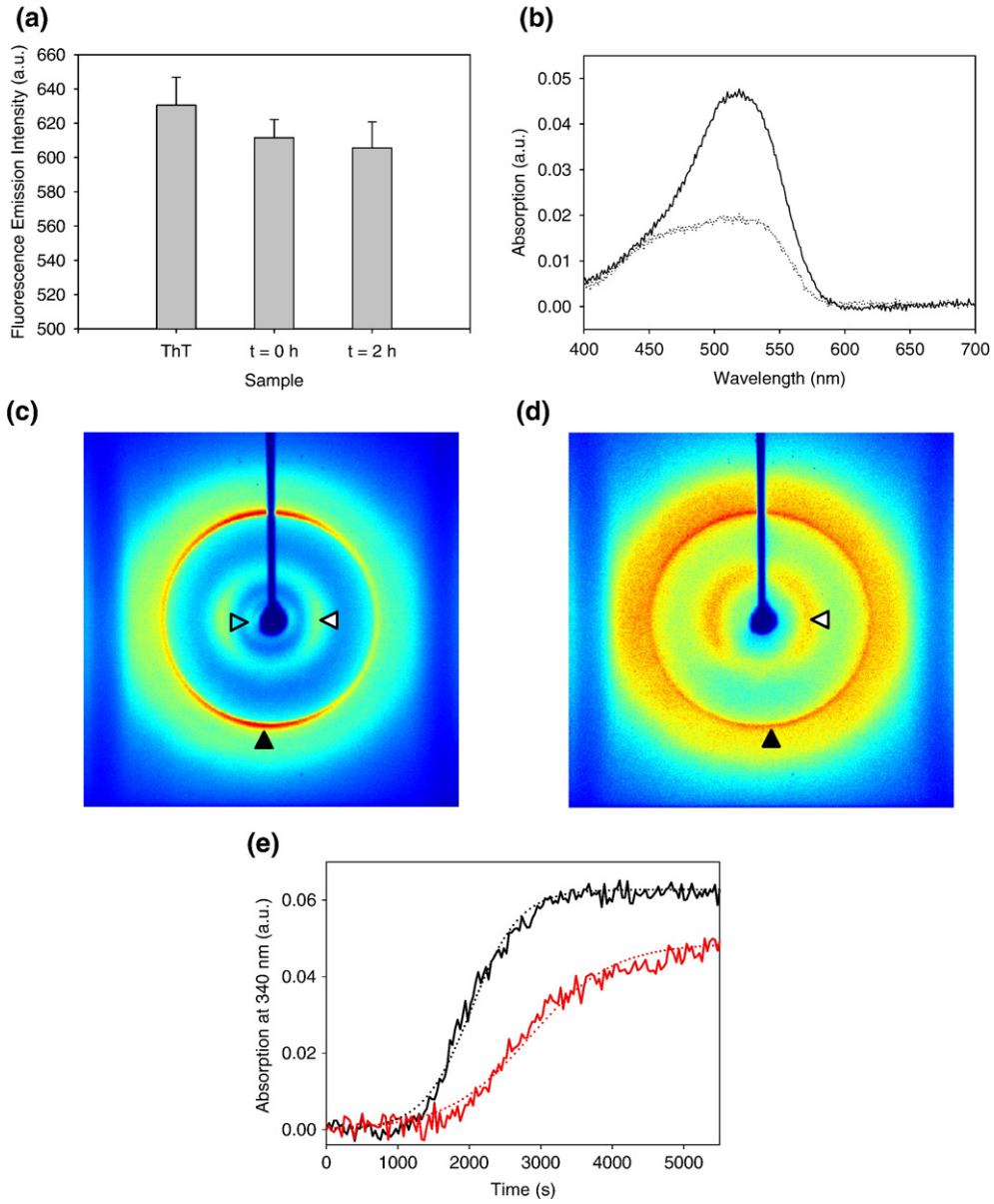

Figure 2. Characterisation of αB-crystallin fibril formation at pH 7.4 with guanidine hydrochloride. (a) ThT fluorescence emission intensity in the presence of αB-crystallin before ($t = 0$ h) and after fibril formation ($t = 2$ h). *a.u.*, arbitrary units. (b) Absorbance spectra of CR in the presence of αB-crystallin before (continuous line) and after fibril formation (dotted line). (c) and (d), X-ray fibre diffraction patterns of αB-crystallin and R120G αB-crystallin fibrils, respectively; meridional reflection at 4.7 Å (filled black triangle), equatorial reflection at 10.0 Å (filled white triangle), and, equatorial reflection at 23 Å (open triangle). (e) Data showing the kinetics of aggregation as determined from turbidity studies of wild-type (black continuous line) and R120G αB-crystallin (red continuous line) are overlaid (filled circles). Data were fitted to three parameter sigmoidal curves (black and red dotted lines), giving apparent rate constant values for the growth phase of aggregation to be 0.178(±0.005) min^{-1} and 0.103(±0.004) min^{-1} for the wild-type and mutant protein, respectively.

Identification of non-core regions of αB-crystallin amyloid fibrils by ^{1}H NMR solution spectroscopy

The solution state 1D ^{1}H NMR spectrum of αB-crystallin in the presence of 1 M guanidine deuterochloride (GdnDCl) (pH 7.4) is shown in Figure 3(a). Under these conditions αB-crystallin maintains its highly aggregated native-like state.[39] As described elsewhere,[28] the 12 solvent exposed amino acids at the C-terminus of αB-crystallin are highly mobile having flexibility comparable to a free peptide of this length,[40] leading to resolved and assignable NMR resonances from this portion of the protein despite the high molecular mass (average ~600 kDa[27]) of the aggregate. The ^{1}H NMR spectrum of native-like αB-crystallin in 1 M GdnHCl is identical to that of αB-crystallin in the absence of denaturant,

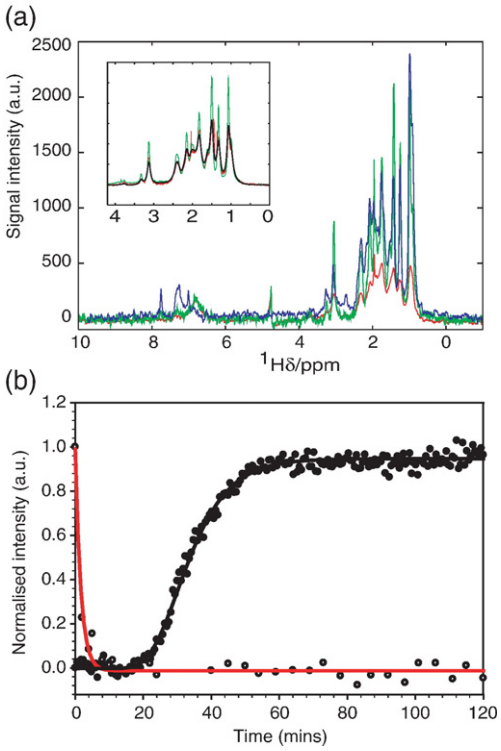

Figure 3. 1D ^{1}H NMR spectra of the native-like and fibrillar αB-crystallin at pD 7.4 with guanidine deuterochloride. (a) A comparison of 1D ^{1}H NMR spectra acquired for native-like (green trace) species *versus* fibrils (red trace). Real-time 1D ^{1}H NMR spectra were acquired during the course of fibril assembly; the first spectrum was acquired within 1 min of the sample being placed in the spectrometer at 60 °C (blue trace). Inset (a), a comparison of 1D ^{1}H NMR spectra acquired for native-like species (green) *versus* fibrils (red) where spectra were normalised for signal intensity and concentration. Subsequently, the normalised native-like protein spectrum (green) was further adjusted by applying line broadening (20 Hz) to achieve a spectrum (black) to match that observed for the fibrils (red). (b) Calculated integrals of the signal intensity from the aliphatic region of 1D ^{1}H NMR spectra (0–6 ppm) acquired during fibril formation (open circles) was fitted to a single exponential (red continuous line) decaying with a half-life time of 69(±6) s. Data showing the kinetics of aggregation as determined from turbidity studies are overlaid (filled circles). Data were fitted to a sigmoidal curve (black continuous line) and normalised.

showing that the presence of this concentration of GdnHCl does not detectably affect the flexibility of the NMR-observable C-terminal extension.

Remarkably, the ^{1}H NMR spectrum of purified αB-crystallin fibrils is very similar to that of the native-like protein, with resonances from the C-terminal extension being observable at chemical shifts close to those corresponding to a random coil state, except that the spectrum is significantly broadened in the fibrillar state (Figure 3(a)). To illustrate this point, the native-like and fibril spectra were first normalised for their total signal intensity (Figure 3(a), inset), and the free induction decay of the native-like state multiplied by an exponential function that corresponds to line broadening by 20 Hz; the resulting spectrum is effectively identical to that of the protein in its fibrillar state that was processed with a 2 Hz exponential function (Figure 3(a), inset). This result strongly suggests that the same 12 amino acid residues observable in the native state correspond to those observed in the fibrillar state and that the transverse relaxation time (T_2) values of the ^{1}H NMR resonances arising from the fibrillar species are approximately ten times shorter than those of the native-like sample. This finding indicates the effective correlation time (τ_c) of the C-terminal residues in the fibril is significantly longer than that for in the native-like aggregate. The increase in the apparent τ_c values could have its origin in one of a combination of two factors: the reduced tumbling of the fibrils compared to the native protein, or a reduced conformational flexibility of the C-terminal extension itself. The random coil chemical shifts of the resonances of the C-terminal residues in both the native and fibril state indicate that the perturbed relaxation behaviour is unlikely to be associated with the generation of significant persistent structure in this region.

Diffusion measurements can be used to estimate the effective hydrodynamic radius of a species in solution,[41,42] and NMR methods were used here to determine diffusion coefficients for the native-like and fibrillar states of αB-crystallin. The diffusion coefficient was measured to be $3.8(\pm0.2)\times10^{-7}$ cm^2 s^{-1} for the native-like state (see Materials and Methods for experimental details). Approximating the protein complexes as hard spheres and using the Stokes–Einstein equation, the corresponding hydrodynamic radius for the native-like state is approximately 5.8(±0.4) nm. This value is consistent with results from cryo-EM data (radii of 4–9 nm, with an average of 6.5 nm)[30,43] for the native αB-crystallin aggregate. The diffusion coefficient was measured to be $2.8(\pm0.2)\times10^{-7}$ cm^2 s^{-1} for the fibrillar species, which is indicative of a larger species in solution than that of the native-like state.

In summary, the NMR data show that the 12 amino acid C-terminal extension of αB-crystallin can be observed by solution ^{1}H NMR spectroscopy not only for the protein in its native-like state but also in its fibrillar state, indicating that this flexible region protrudes from the main cross-β-sheet amyloid core of the fibrils.

The kinetic timecourse for αB-crystallin amyloid fibril formation

For comparative purposes, human αB-crystallin was monitored throughout the process of amyloid fibril formation by real-time 1D ^{1}H NMR spectroscopy under the same conditions employed for the turbidity assay (Figure 2(e)). Thus, fibril formation by αB-crystallin at 2 mg/ml in pD 7.4 with 1 M GdnDCl, was initiated by elevating the temperature to 60 °C; the first spectrum was acquired within one minute of the sample being placed in the NMR spectrometer. Initially, a large increase in overall signal intensity was observed, attributable to major

global unfolding of the protein. This increase was followed by a rapid decrease in signal intensity as the protein aggregated into its fibrillar state (Figure 3). The measured decrease in signal intensity of the aliphatic region of the spectrum was analysed quantitatively by integrating the spectra (Figure 3(b)), showing that within 5 min no further changes could be identified in the ^{1}H NMR spectra. Interestingly, resonances in the aromatic region of the spectra (ca. 6.8–8.0 ppm) became evident during this time (Figure 3(a)), but disappeared within two minutes; this can be attributed to broadening of resonances in the final fibrillar state, indicating that an intermediate in which some aromatic groups are exposed to solution is formed during the aggregation process. As all aromatic residues are located in the N-terminal domain and in the central regions of the αB-crystallin sequence, it is evident that these regions must unfold prior to fibril formation. Partial unfolding of complex three-dimensional native-like states has been found in other systems to be a prerequisite for amyloid fibril formation.[44,45] The absence of aromatic resonances in the spectrum of the fibrillar state indicates that these aromatic residues become buried by the time fibril formation is complete.

NMR spectra acquired at the beginning and end points of the kinetic assay, corresponding to the native-like and fibrillar states, has allowed the overall signal intensity arising from the observable proton resonances of the C-terminus to be compared quantitatively. This analysis reveals that 43(±6)% of the total number of protons resolved for the native state are visible by NMR spectroscopy in the fibril configuration. Thus, in the course of fibril formation, approximately half of the previously observed native state C-terminal extension protons are incorporated into environment(s) that limit their conformational flexibility, broadening their linewidths beyond a point where they can be observed by conventional solution state NMR spectroscopy.

Comparing these NMR kinetic data with the results of turbidity measurements (Figure 3(b)) shows that after the 1D ^{1}H NMR signal intensity had stabilised (within 5 min), the lag phase observed prior to the measured increase in turbidity associated with aggregation into fibrils continued for another 17 (±1) min. Overall, this suggests that after the rapid formation of a partially unfolded native-like state (observed by NMR spectroscopy), αB-crystallin forms a second intermediate on the pathway to fibril formation. This second intermediate is indistinguishable by NMR from the elongated fibrils, but must either be too small to scatter sufficient light or present at too low a concentration to produce a measurable change in turbidity. It is therefore likely to be a relatively small early oligomeric species formed transiently during the aggregation process.

Prediction of the aggregation propensities of αA-, αB-, and R120G αB-crystallins

The aggregation propensities of the different regions of the sequence of αA-, αB-, and R120G αB-crystallin were predicted by using a modified version of the Zyggregator algorithm[46] (G.G.T. *et al.*, unpublished results†). In this type of prediction a value, Z_{agg}, is associated with each amino acid in the sequence and the resulting profiles for the three crystallins studied here are shown in Figure 4. Z_{agg} values >0 indicate that the sequence is more prone to aggregate than that of a randomly generated sequence with average amino acid composition at a given pH, while it is less prone to aggregate if Z_{agg} values <0.[46] Regions in the N-terminal domain (residues 1–65) and central α-crystallin domain (residues 66–149) of αB-crystallin frequently exhibit positive Z_{agg} values, indicating that these segments of the sequence are prone to self-association *via* intermolecular interactions (Figure 4). In contrast, the 12 residues of the C-terminal region have Z_{agg} values <0, indicating that involvement of this region in an aggregation process is unlikely. This prediction is consistent with conclusions about the structure of the αB-crystallin amyloid fibrils derived in the present work by ^{1}H NMR spectroscopy, demonstrating that the N-terminal and central domains are incorporated in or near to the cross-β core region of the fibrils, or at least are involved in persistent structure, whereas the C-terminal residues are not confined in this way, leaving them to protrude into the solvent in a flexible conformation.

The predicted aggregation profile of αA-crystallin is very similar to that of αB-crystallin, and again the N-terminal and central domains of αA-crystallin are more prone to aggregate than the C-terminal region encompassing the ten residue flexible hydrophilic extension observed in solution state NMR spectra of the native state of this protein.[28] Both αA- and αB-crystallin have slightly higher predicted aggregation propensities at pH 7.4 than at pH 2.0 (Figure 4). Finally, comparison of the overall Z_{agg} score predicted for the R120G αB-crystallin ($Z_{agg}=0.60$) with that of the wild-type αB-crystallin ($Z_{agg}=0.63$) at neutral pH, suggests that the mutant has a slightly decreased propensity to aggregate relative to the wild-type protein (Figure 4(b) and (d)), consistent with the experimentally observed aggregation kinetics of these proteins, as measured by turbidity studies (Figure 2(e)).

Quantification of the protofilament substructure and manipulation of αB-crystallin fibril morphology

TEM studies show that αB-crystallin fibrils formed at pH 7.4 possess a wavy, and apparently branched morphology (Figure 5(a) and (b)), with an appearance that suggests that the individual protofilaments of which the fibril is composed can separate from each other under these conditions, i.e. they are weakly interacting. In order to investigate in

† http://www-vendruscolo.ch.cam.ac.uk/zyggregator.php

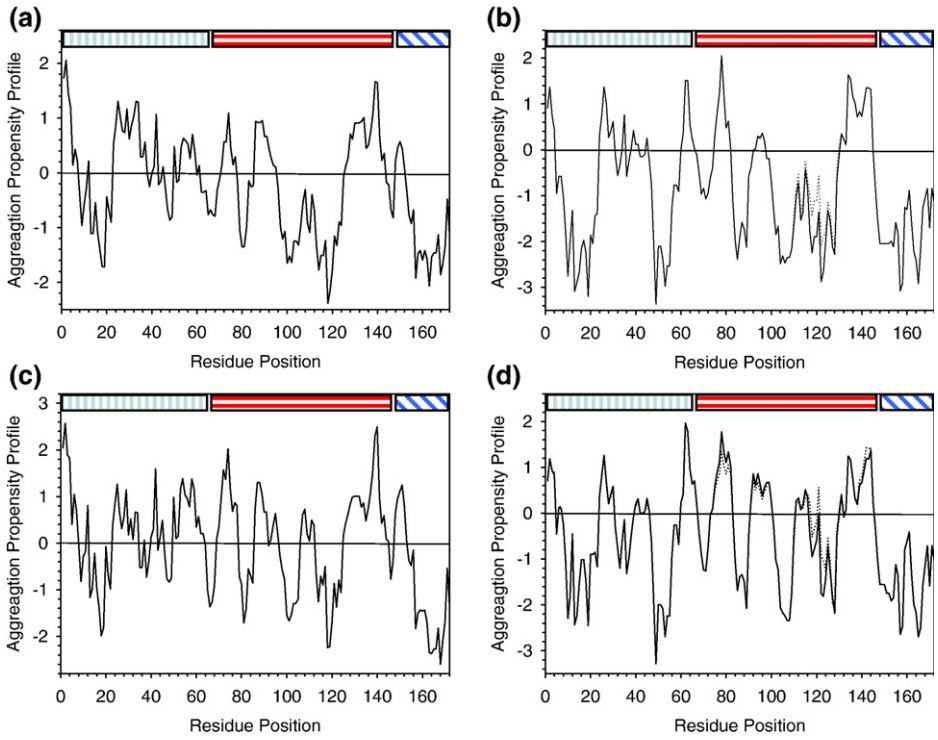

Figure 4. Aggregation profiles of αA-, αB-, and R120G αB-crystallin. Aggregation profiles generated for: (a) αA-crystallin at pH 2.0; (b) αB-crystallin (continuous line) and R120G αB-crystallin (dotted line) at pH 2.0; (c) αA-crystallin at pH 7.4; (d) αB-crystallin (continuous line) and R120G αB-crystallin (dotted line) at pH 7.4. Indicated on the panels as rectangular boxes are the N-terminal domain (vertical line pattern), the central "α-crystallin" domain (horizontal line pattern), and C-terminal domain (diagonal line pattern) encompassing the flexible C-terminal region.

more detail the interactions between protofilaments controlling this process, we titrated the fibril solutions to a range of pH values. For example, aliquots from branching fibril solutions (10 mg/ml, pH 7.4; Figure 5(a) and (b)) were diluted to 1 mg/ml and adjusted to pH 2.0, and the samples then prepared immediately for TEM and AFM analyses. Images (Figure 5(c)–(f) and Figure 6(b)) of fibrils after this treatment reveal a dramatic separation of the component protofilaments into assemblies resembling loosely associated plaits. Following further sample dilution (0.1 mg/ml), and incubation at pH 2.0 for a period of 14 days additional morphological changes can be distinguished by AFM revealing complete unravelling and dissociation of the protofilaments from the fibrils (Figure 6(c)). This process was accompanied by breakage of the fibrils (ca 2–10 μm in length) into multiple shorter protofilaments approximately 200 nm in length (Figure 6(c)). Dilution alone, without changing the pH of the solution, was found not to be sufficient to induce such changes indicating that the reduction in pH is the critical factor.

The AFM data were then analysed quantitatively to provide statistical distributions of the fibril dimensions,[47] enabling three types of structure to be identified (Table 1). There are (1) individual protofilaments, observed not just as open chains but also as closed loops (Figure 6(c)); (2) loosely associated plaits (Figure 6(b)); and (3) mature branched fibrils (Figure 6(a)). The height data, summarised in Table 1, reveal that the average diameter of the dissociated protofilaments (2.2(±0.4) nm, Figure 6(c)) is the same, within the standard deviations, as the protofilament diameter of the loosely associated plaits (2.9(±0.7) nm; Figure 6(b)), and indeed to single protofilaments of other amyloid systems. These data are consistent with the notion that the individual protofilaments are a dissociated form of the plaits that appear to be composed of two protofilaments (Figure 6(b)). We cannot observe individual protofilaments in the mature fibrils, but the diameters (10.0(±1.7) nm) suggest that they are perhaps assembled from a doublet of protofilament pairs, i.e. four protofilaments in total.

The morphological change from the mature branched fibrils (pH 7.4) to the plaits (pH 2.0) was found to be reversible, as assessed by TEM; readjusting solutions at pH 2.0 back to pH 7.4 within 3 h of the original pH jump stimulated re-assembly of the plaits (Figure 5(c)–(f)) into mature branching fibrils indistinguishable from those in Figure 5(a) and (b). However, once the fibrils were observed to dissociate completely into individual protofilaments and also fracture (Figure 6(c)) after two weeks of incubation at pH 2.0, subsequent readjustment of the solution back to pH 7.4 did not induce reassembly into the higher-order mature branching fibrils, as assessed by TEM, at least on the timescales of our study.

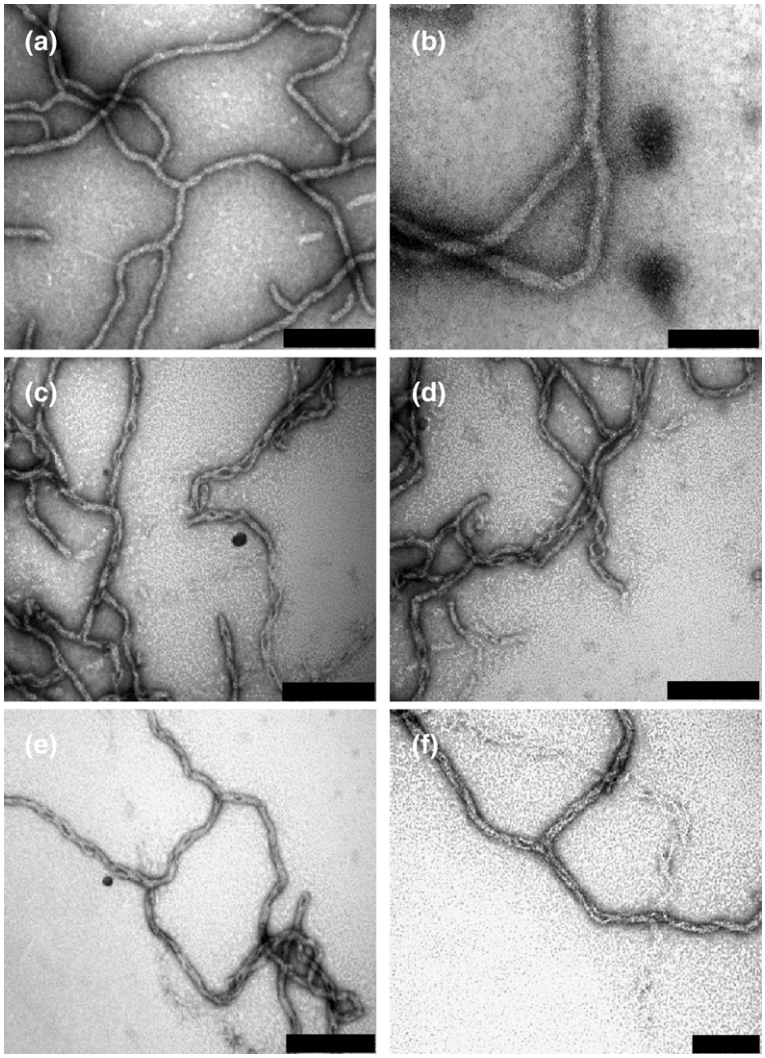

Figure 5. Dissociation of αB-crystallin fibrils. TEM images of fibrils prepared with GdnHCl at pH 7.4, (a)–(b), and following a ten-fold dilution into a pH 2.0 solution (c)–(f). The scale bar represents 200 nm in (a), (c), (d) and (e), and 100 nm in (b) and (f).

Characterisation of amyloid fibrils formed by human recombinant αA-, αB-crystallin, and R120G αB-crystallin at pH 2.0

Human recombinant αB-crystallin was subjected to partially denaturing conditions at acidic pH, and assessed for its propensity to form amyloid fibrils, employing conditions reported previously to induce fibril assembly by bovine α-crystallin.[12] αB-Crystallin was dissolved at 10 mg/ml in 10% (v/v) TFE, 90% (v/v) H_2O, at pH 2.0, and incubated at 60 °C for 24 h prior to examination by TEM and AFM. The resultant fibrils of αB-crystallin show a short and curly morphology, ranging from 40 nm to several hundred nanometres in length. Moreover, closed loops with diameters ranging from 40 nm to 230 nm were frequently observed (e.g. Figure 6(d) and Figure 7(a)). Statistical analysis of AFM images of these fibrils revealed average heights of 3.0(±0.8) nm (Table 1). Overall, the morphologies and dimensions of αB-crystallin fibrils formed at pH 2.0 with TFE (Figure 6(d)) appear very similar to those formed at pH 7.4 in the presence of GdnHCl and for which the pH had subsequently been adjusted to pH 2.0 (Figure 6(c)). The interaction of αB-crystallin fibrils formed at acidic pH with the dyes CR and ThT was similar to that of αB-crystallin fibrils formed at pH 7.4 as described above (cf. Figure 2(a) and (b)), i.e. no positive interaction with ThT was observed, and both native-like and fibril conformations had a positive interaction with CR (data not shown). For comparative purposes, the amyloid-forming propensities of αA- and R120G αB-crystallin were also investigated at pH 2.0, revealing that these subunits form amyloid fibrils of a similar morphology to those of wild-type αB-crystallin (Figure 7(b) and (c)). X-ray fibre diffraction experiments indicate that both αB- and R120G αB-crystallin fibrils formed at pH 2.0 exhibit a cross-β-pattern with anisotropic reflections at 4.7 Å and 10.0 Å, characteristic of the cross-β structure of amyloid fibril formation (Figure 7(d) and (e)).

Discussion

The sHsps αA-, and αB-, and R120G αB-crystallin form amyloid fibrils

The sHsp αB-crystallin is renowned for its protective chaperone ability.[16,29] *In vivo*, αB-crystallin is stress-inducible, and its up-regulation is associated with a number of clinical disorders including

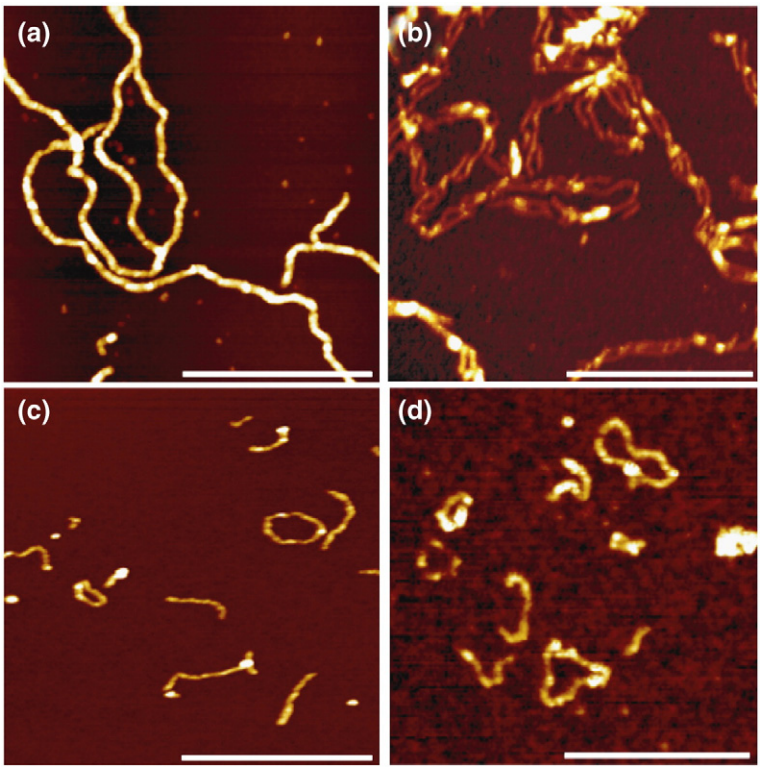

Figure 6. AFM images of αB-crystallin fibrils. AFM images of: (a) fibril solutions prepared at pH 7.4 with GdnHCl, then, following a tenfold (b), or one 100-fold (c), dilution into a pH 2.0 solution; (d) αB-crystallin fibrils prepared with TFE at pH 2.0. The scale bar represents 500 nm.

Alexander's disease, Lewy body disease, oncogenesis, and also conditions linked to fibril deposition such as Alzheimer's disease, Creutzfeldt–Jakob disease, scrapie, and Parkinson's disease.[18,48] Furthermore, it is a crucial protein in the prevention of cataract formation.[2,17,18] αB-Crystallin is frequently found co-localised with amyloid plaques *in vivo*[18] and is effective *in vitro* at inhibiting amyloid fibril formation by a wide range of target proteins, including amyloid β peptides.[49,50] The sequences of αA- and αB-crystallin have an amphiphilic character, a property likely to be crucial to their function as molecular chaperones.[17] The hydrophobic regions in the N-terminal and central α-crystallin domain are thought to interact with partially unfolded target proteins displaying exposed hydrophobic patches,[51] and the flexible hydrophilic C-terminal extension to play a role in maintaining the solubility of complexes of the chaperone with target proteins.[17,29,52] Indeed, it is under conditions of stress *in vivo* where the functional chaperone activity of αA- and αB-crystallin is most likely to be in demand. We investigated here the effects of partial denaturation and heat stress on human recombinant αA-, αB-, and the mutant R120G αB-crystallins, *in vitro* and demonstrate that these conditions can lead to prompt self-assembly into amyloid fibrils. These results suggest that a fine balance may be at play *in vivo* between a natively aggregated functional sHsp state and a misfolded aggregate in the form of amyloid fibrils.

Table 1. Summary of statistical height analysis from AFM studies of αB-crystallin amyloid fibrils

Figure	Morphology	Mean height and standard deviation (nm)
6(a)	Mature branched fibrils	10.0±1.7
6(b)	Protofilament pairs as plaits, and their individual protofilaments	4.0±1.7 2.9±0.7
6(c)	Individual protofilaments, both open chains and closed loops	2.2±0.4
6(d)	Individual protofilaments, both open chains and closed loops	3.0±0.8

For αB-crystallin under each set of conditions (see Figure 6(a)–(d)) individual fibrils were traced from the AFM topographic data using an algorithm described.[47] A statistical height distribution histogram was generated in each case and the mean fibril heights and standard deviation values are summarised here.

The sequences of αA- and αB-crystallin will play an important role in maintaining this balance in favour of their native states *in vivo* under normal physiological conditions. The results of a theoretical analysis of the aggregation propensity of αB-crystallin, calculated from the physico-chemical properties of its amino acid sequence in given environments, show that the C-terminal extension is likely to be highly resistant to aggregation. Moreover, NMR experiments reveal that the 12 C-terminal residues of the protein are excluded from the highly structured core of the αB-crystallin amyloid fibrils. In an unrelated amyloid fibril-forming system, lysozyme,[53] it has been shown through limited proteolysis experiments that the core structure of the fibrils is formed by assembly of the most highly aggregation-prone regions of the sequence. Similarly, the inclusion and exclusion of particular regions of the αB-crystallin polypeptide chain in the fibril, as found experimentally, correlate very well with the predicted aggregation propensity of its sequence.

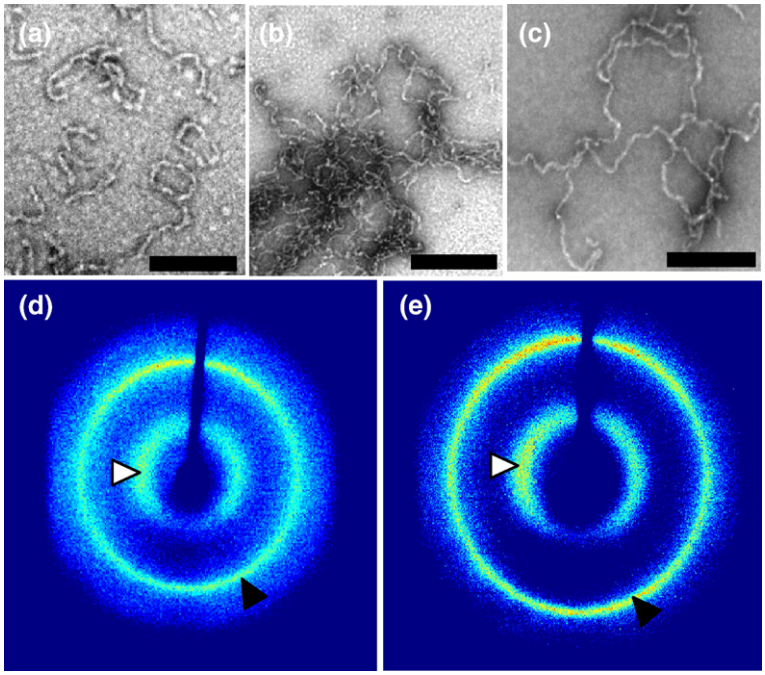

Figure 7. Fibril formation by αA-, αB-, and R120G αB-crystallins at pH 2.0 with TFE. TEM images of fibrils formed from: (a) αB-crystallin; (b) αA-crystallin; and (c) R120G αB-crystallin. The scale bar represents 200 nm. (d) and (e) X-ray diffraction pattern of (d), αB-crystallin and (e), R120G αB-crystallin fibrils; meridional reflection at 4.7 Å (filled black triangle); equatorial reflection at 10.0 Å (filled white triangle).

Dynamic αB-crystallin protofilament assemblies and morphological manipulations

αB-Crystallin fibrils display an unusual apparently branched morphology at pH 7.4 (Figures 5(a), (b) and 6(a)). In contrast to other reported examples of amyloid fibrils where splaying into separate protofilaments has been visualised,[54,55] the loosely associated αB-crystallin fibrils remain stable for months at room temperature, and do not appear to be the precursors of a more mature tightly wound fibril. The elastic cost of protofilament helical assembly and of the resulting inter-protofilament interactions may be low, leading to loosely associated protofilaments that are readily unravelled and restructured. Indeed, the present study indicates that very large morphological changes can be provoked by adjusting the pH of solutions containing αB-crystallin amyloid fibrils. These processes were observed with particular clarity by AFM, and we employed statistical height analysis to resolve and quantify different levels of protofilament substructure for the αB-crystallin fibril system (summarised in Figure 8). Thus, for example, decreasing the pH of a mature "branching" fibril solution from pH 7.4 to pH 2.0 can be seen to trigger dissociation from assemblies of multiple protofilaments to generate protofilaments pairs. This first dissociation step is rapid and reversible, and is likely to result from the considerable change in the overall charge of the protein, from −1 to +34 between pH 7.4 and pH 2.0; the change localised within the 12 amino acid C-terminal extension (E164 to K175) is from zero to +3. Such large changes in charge are very likely to be the origin of repulsive electrostatic interactions between the protofilaments and hence of the dramatic disruption of the multiple protofilament assemblies (Figure 8).

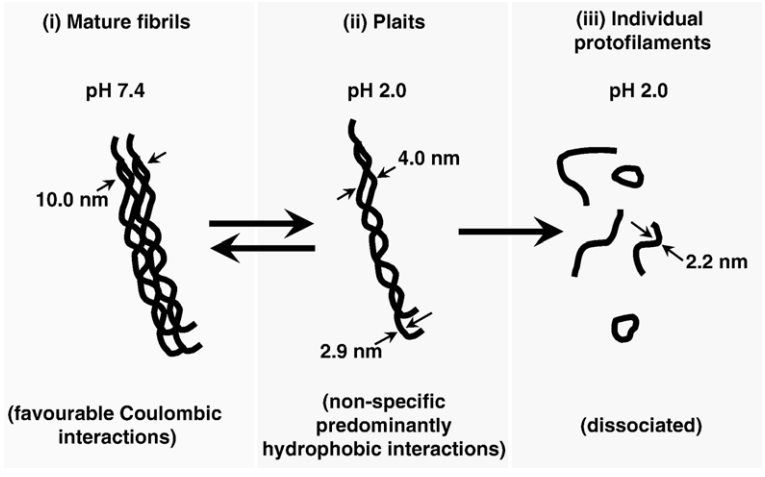

Figure 8. Putative models to show hierarchical assembly of protofilaments of αB-crystallin amyloid fibrils based on data from AFM imaging and statistical height analysis. Model designed to suggest protofilament substructure of αB-crystallin amyloid fibrils, with an indication of inter-protofilament interactions: (i) mature fibrils (cf. Figure 6(a)) with mean heights of 10.0(±1.7) nm; (ii) dissociating fibrils (cf. Figure 6(b)) with mean overall heights of 4.0(±1.7) nm and individual protofilaments with mean heights of 2.9(±0.7) nm; and (iii) dissociated lone protofilaments (cf. Figure 6(c)) with mean heights of 2.2(±0.4) nm.

The protofilament pairs discussed above (Figure 6(b)) were found to dissociate further into individual protofilaments after longer periods of time in dilute solution (Figure 6(c)). The shorter length distribution of these single protofilaments from the fibrillar structures indicates an increased susceptibility to breakage in comparison with the higher order assemblies of protofilaments; this finding is consistent with the smaller diameter of the protofilaments, a feature that leads to an increased rate of internal fracturing.[56] Once the fibrils had separated and then fractured into shortened single protofilaments of approximately 200 nm in length (cf. Figure 6(c)), reassembly into long mature fibrils comprised of multiple bundles of protofilaments (ca 2–10 μm in length; cf. Figure 6(a)) was not observed to occur when the solutions were readjusted to pH 7.4. This finding can be rationalised by the fact that the kinetics of the end-to-end inter-molecular reassociation of the lone protofilaments are likely to be determined by the small rotational and translational diffusion coefficients of the individual protofilaments in the suspension, leading to the system becoming kinetically trapped in an energetically less favourable state where the inter-filament interaction energy is lost. In addition, the extra entropy of the dissociated state is likely partly to counterbalance the enthalpic energy penalty associated with conversion of the fibrils to this state.

In contrast to such inter-molecular interactions, intra-molecular end-to-end association of the short individual protofilaments appears to be highly favorable (Figure 6(c)), as AFM images reveal the presence of substantial numbers of closed loops appearing to form spontaneously. Qualitatively, the probability of a single fibril joining end-to-end to form a closed loop will be high if the fibril is sufficiently flexible and of appropriate length for the ends regularly to find themselves in close proximity.[57] Indeed, the present study exemplifies the favourable nature of loop formation when such fibril morphologies are adopted. Loop formation has been reported previously for other amyloid forming systems,[58] and it has been suggested that very small amyloid loops, or "pores", may represent a particularly toxic form of early aggregate species.[59]

It is interesting to note that a very similar fibril morphology for αB-crystallin can be achieved *via* two distinct experimental routes: the single protofilament, in the form of both open flexible chains and closed loops, is observed (i) after fibril formation in the presence of GdnHCl at pH 7.4, followed by subsequent dilution into a pH 2.0 solution, and also (ii) after fibril formation at pH 2.0 in the presence of TFE. This observation again suggests that charge plays a key role in such conformational transitions.

Conclusions

This study has revealed that the hydrophilic C-terminal extension in αB-crystallin has a low propensity to aggregate and protrudes in a flexible conformation from the cross-β-amyloid core formed by this protein. This result is in accord with theoretical analysis of the propensity of different regions of the sequences to aggregate made on the basis of the physico-chemical properties of an amino acid sequence in a particular environment.[46,60,61] Moreover, we demonstrate that it is possible to alter the position of equilibrium between different dynamic αB-crystallin protofilament assemblies and dictate the resultant amyloid fibril morphology. It is particularly interesting that a chaperone that otherwise is involved in the prevention of aggregation, can itself convert into such fibrils. This finding adds further evidence to the concept that the ability of polypeptide chains to assemble into amyloid fibrils is a generic property although the propensity to do so is determined by the intrinsic properties of a given sequence.[1] In addition, however, this study suggests that there is a delicate balance in α-crystallin between the functionally important aggregation of a protein in its native state and the potentially pathogenic assembly of misfolded proteins into the amyloid structure.

Materials and Methods

Expression and purification of human recombinant αA-, αB-, and R120G αB-crystallins

The vector pET23d(+) containing the gene for expression of human αA-crystallin, was a gift from Professor J. M. Petrash (Washington University, St. Louis, USA), the vector pET24d(+) (Novagen, Madison, USA) containing the gene for expression of human αB-crystallin was a gift from Professor W. de Jong and Professor W. Boelens (University of Nijmegen, Netherlands), and the vector pET20b(+) (Novagen, Madison, USA) containing the gene for expression of human R120G αB-crystallin, was a gift from Professor J. Horwitz (University of California, Los Angeles, USA). Human recombinant αA-, αB-, and R120G αB-crystallins were expressed and purified as described (αA-crystallin,[62] αB-crystallin,[63] R120G αB-crystallin[64]).

Formation of amyloid fibrils

Formation from human recombinant αAB-, αB-, and R120G αB-crystallins at pH 7.4 with 1 M guanidine hydrochloride

Human recombinant αA-, αB-, and R120G αB-crystallins were dissolved at 1.0–10 mg/ml in 0.1 M phosphate buffer (pH 7.4), and incubated at 60 °C for 2 h with 1 M GdnHCl to form amyloid fibrils. Fibril formation was accompanied by a slight increase in opacity and viscosity of the solution as observed by eye. Lower incubation temperatures were not found to be sufficient to induce amyloid fibril assembly *in vitro* within 24 h; for example, after incubation of αB-crystallin at 37 °C for one week in the presence of 1 M GdnHCl (pH 7.4) we observed roughly spherical aggregates by TEM, typical of native α-crystallin.[65] Native R120G αB-crystallin is prone to truncation[64] and for this reason we assessed whether this mutant protein suffered any degradation during amyloid assembly. Formation, purification, and solubilisation of R120G αB-crystallin fibrils, followed by subsequent analysis by mass spectrometry reveals a single species corresponding to the full-length protein.

Formation from human recombinant αB-crystallin at pH 7.4 with TFE

Human recombinant αB-crystallin was dissolved at 1.0 mg/ml in 10% (v/v) TFE, 0.1 M phosphate buffer (pH 7.4), and incubated at 60 °C for 2 h.

Formation from human recombinant αA-, αB-, and R120G αB-crystallin at pH 2.0

Human recombinant αA-, αB-, and R120G αB-crystallins were dissolved at 1.0–10 mg/ml in 10% (v/v) TFE, adjusted to pH 2.0 with HCl, and incubated at 60 °C for 4 h.

Characterisation of human recombinant αA-, αB-, and R120G αB-crystallin amyloid fibril formation

Turbidity assay/aggregation kinetics

Human recombinant αB-crystallin and R120G αB-crystallin were dissolved at 2 mg/ml in 0.1 M phosphate buffer (pH 7.4) with 1 M GdnHCl, filtered through a 0.2 μm filter and incubated at 60 °C for 2 h. The change in turbidity/light scattering of a 0.1 ml solution was monitored by measuring the absorbance at 340 nm using a Fluostar Optima plate reader (BMG Labtechnologies, Australia).

Transmission electron microscopy (TEM)

Formvar and carbon-coated nickel electron microscopy grids were prepared for this study by the addition of 2 μl of protein sample at a concentration of 1 mg/ml. The grids were then washed with 3×10 μl H_2O and negatively stained with 10 μl of uranyl acetate (2% (w/v); Agar Scientific). The grids were dried with filter paper between each step. Samples were viewed under 20–125 k magnifications at 120 kV excitation voltages using a Philips CM100 transmission electron microscope.

Congo red assays

Fresh solutions of CR[31,33] in 5 mM potassium phosphate buffer containing 150 mM NaCl (pH 7.4), were passed through a 0.2 μm filter immediately before use. The CR solutions were added to 100 μg/ml protein solutions to a final dye concentration of 0.5 μM, and the samples vortexed for 15 s. The absorption spectrum of each sample was recorded from 400 nm to 700 nm on a Varian Cary Bio UV-visible spectrophotometer using 1 cm path length quartz cuvettes and corrected for contributions from buffer and protein. The spectrum of CR alone was compared with that of CR solutions in the presence of protein. A red shift of the absorption band toward 540 nm was taken to be indicative of the formation of amyloid structures.

Thioflavin T fluorescence

The spectrum of ThT alone was compared with that of protein solutions (0.05–1.0 mg/ml) containing ThT at a final dye concentration of 10 μM in 50 mM glycine–NaOH buffer (pH 9.0). Fresh solutions of ThT were passed through a 0.2 μm filter immediately before use. A Fluostar Optima plate reader (BMG Labtechnologies, Australia) was used to record the spectra in Greiner black μClear 96 microwell plates (Interpath Services, Australia) using a sample volume of 100 μl in each well (λ_{Ex}=440 nm; λ_{Em}=490 nm). An increase in the fluorescence emission intensity at 490 nm was taken to be indicative of amyloid formation.[32] The average fluorescence emission intensities and standard error values were calculated from a total of at least four readings for each sample.

X-ray fibre diffraction

Fibril samples (formed at 10 mg/ml (pH 7.4) with 1 M GdnHCl) were buffer exchanged to remove salts and both wild-type and R120G αB-crystallin fibril solutions were ultracentrifuged at 90,000 r.p.m. for 1.5 h (316,613 r.c.f.) in a Beckman Coulter Optima TL-X ultracentrifuge using a TLA 100 rotor. The supernatant was subsequently carefully removed, and the fibril pellet in each case was re-suspended in a volume of water so as to maintain the original protein concentration. Wild-type and R120G αB-crystallin samples for X-ray fibre diffraction were prepared by air-drying an ultracentrifuge-purified fibril solution between two wax-filled capillary ends using a technique described elsewhere.[66] A small stalk of fibrils protruding from the end of one of the capillaries was obtained, the sample was aligned in an X-ray beam, and diffraction images were collected using a Rigaku CuKα-rotating anode source (wavelength, 1.5418 Å) and an R-AXIS IV image plate X-ray detector. Images were analysed and radially integrated to generate 1D scattering patterns using Matlab code written in-house,[66] to obtain accurate reflection positions. Wild-type and R120G αB-crystallin fibril solutions prepared at pH 2.0 in the presence of TFE were also examined by X-ray fibre diffraction. In this case, samples were prepared directly from 12 μl of fibril stocks without ultracentrifugation and buffer exchange.

Fibril purification

αB-Crystallin fibril solutions were ultracentrifuged at 90,000 r.p.m. for 1.5 h (316,613 r.c.f.) in a Beckman Coulter Optima TL-X ultracentrifuge using a TLA 100 rotor. The supernatant was subsequently carefully removed, and the fibril pellet was re-suspended in the volume of buffer required to regenerate the original protein concentration.

Atomic force microscopy of αB-crystallin amyloid fibrils at pH 2.0 and pH 7.4 and manipulation of the amyloid morphology

Atomic force microscopy (AFM)

Solutions of crystallins (20 μl, 0.05–10 mg/ml) were deposited on to freshly cleaved mica substrates (Agar Scientific Ltd, Stansted, Essex, UK) and air-dried. Topographic data were then acquired either with a Molecular Imaging Pico Plus microscope (Figure 6(a)–(c)) or a Dimension 3100 SPM (Veeco Instruments Inc., Woodbury, NY, USA) in conjunction with a Nanoscope IV control system (Figure 6(d)), both operating in tapping mode. Ultrasharp Micromasch silicon and silicon nitride cantilevers (NCS36 or $NSC_{12}/Si_3N_4/50$) were used at resonant frequencies between 150 kHz and 225 kHz.

AFM height analysis

Individual fibrils were traced from the AFM topographic data using an algorithm described,[47] and the height of the fibril relative to the background was

evaluated for points located on the fibril backbone. For all cases, 600 to 3000 individual height measurements spread over more than 40 different fibrils were considered for each sample.

Sample preparation for AFM studies

Solutions of αB-crystallin fibrils were prepared by dissolving the protein at 10 mg/ml in 0.1 M phosphate buffer (pH 7.4), and incubating at 60 °C for 2 h with 1 M GdnHCl. Two separate aliquots were removed from this fibril solution and treated as follows. (1) A 20 μl aliquot was diluted tenfold and adjusted to pH 2.0 with HCl, and samples were prepared immediately for TEM and AFM analysis. Within 3 h, this pH 2.0 solution was readjusted to pH 7.4 with NaOH and samples were prepared immediately for TEM analysis. (2) A 20 μl aliquot was removed and diluted 100-fold into water adjusted to pH 2.0 with HCl, and incubated at room temperature for two weeks before samples were prepared for AFM analysis. Fibrils were then pelleted by centrifugation and resuspended in 1 M phosphate buffer (pH 7.4), with 1 M GdnHCl, and incubated at room temperature for one week before samples were prepared for TEM analysis. Sample concentrations were separately optimized for AFM and TEM imaging following dilution.

Nuclear magnetic resonance (NMR) spectroscopy

αB-Crystallin was dissolved at 2 mg/ml in 0.1 M phosphate buffer (pD 7.4) (100% (v/v) ^2H_2O) to a final volume of 0.2 ml, with 1 M GdnDCl for investigation by NMR spectroscopy. Fibrils were formed by incubating the solution at 60 °C for 2 h. The fibrils were purified by ultracentrifugation as described above. Under these centrifugation conditions, the native state was not found to form pellets, and therefore purified fibril samples were subsequently re-purified by the same method several days later. No material was found in the second supernatant, demonstrating that the fibrils do not dissociate into monomeric species on this timescale. No visible sedimentation of the fibrils to the bottom of the NMR tube was observed.

Both the native and the fibrillar states were characterized by solution state NMR spectroscopy. One-dimensional (1D) ^{1}H NMR spectra were acquired using a 500 MHz TCI Bruker spectrometer with a cryo-probe using WATERGATE solvent suppression[67] at 27 °C, with a sweep width of 8012 Hz, and a relaxation delay of 1 s. Once formed and purified no change in the overall intensity of NMR resonances or their chemical shifts was observed over a 140 h period, demonstrating the stability of the fibril samples. The total resonance intensities of both the native and fibrillar samples were normalized by concentration, as determined by UV-Vis measurements, to allow comparison of the total signal intensity observed in the two states. Diffusion data were acquired using a stimulated echo pulse sequence with sinusoidal gradients, and with $\delta = 5.4$ ms (duration of gradients) and $\Delta = 300$ ms (delay between gradients). Spectra were acquired varying the gradient strength G, and fitted to $S_i = S_0 \exp(-G_i^2\gamma^2\delta^2 D T(\Delta - \delta/3))$, where S_0 is the signal intensity at $G = 0$, and S_i the signal intensity for G_i, and γ is the gyromagnetic ratio.[68]

A kinetic assay was performed to monitor the changes in 1D ^{1}H spectra throughout the time course of amyloid fibril formation and to compare the overall change in signal intensity of the native and fibrillar states, using a broadband ATM Bruker 500 MHz NMR spectrometer. The native state was first characterized at 27 °C by acquisition of a 1D NMR spectrum. The magnet was shimmed and calibrated at 60 °C on a sample of 1 M GdnDCl, 0.1 M phosphate buffer (100% ^2H_2O) at pD 7.4 filtered through a 0.2 μm syringe filter. The native state sample of αB-crystallin in the same buffer that had been kept at room temperature was subsequently inserted into the magnet and 32-scan ^{1}H 1D spectra were acquired consecutively for 2 h at 60 °C, with each spectrum taking 64 s to acquire. Once fibril formation was complete, the sample was returned to 27 °C to allow direct comparison of signal intensity between the newly formed fibrillar state and the native state. All spectra were processed similarly.

Prediction of the aggregation propensity profiles

The aggregation propensities of the different regions of the protein sequences were calculated by using a modified version of the Zyggregator algorithm[46] (G.G.T. *et al.*, unpublished results‡). This approach is based on the observation that the physico-chemical properties of the amino acids can be used to calculate the changes in the aggregation propensities of polypeptide chains upon mutation,[60] as well as the overall aggregation propensities of peptides and proteins.[61] This idea was further applied to calculate the intrinsic propensities for aggregation of the different regions of unstructured polypeptide chains[46] and it has been recently extended to partially structured proteins (G.G.T. *et al.*, unpublished results).

Acknowledgements

We thank Professor Mark Walker, University of Wollongong, for helpful discussions and overseeing the expression and purification of αA-, αB-, and R120G αB-crystallin. We thank Professor Mark Welland, Drs Margaret McCammon, Glyn Devlin, and Anne Dhulesia, University of Cambridge, and Dr Bruce May, University of Adelaide, for helpful discussions. We thank Dr Lyn Waterhouse (University of Adelaide) for assistance with TEM, and Damaris Amman and Dr Rachel McKendry (University College London) for assistance with AFM. We acknowledge financial support from a Royal Society International Fellowship (to S. M.), the Medical Research Council (to A. J. B.), the Interdisciplinary Research Collaboration in Nanotechnology (to T. P. J. K.), National Institutes of Health (to J. F. S.), an Australian Postgraduate Award (to T. M. T.), a National Health and Medical Research Council of Australia Peter Doherty Postdoctoral Training Fellowship (to H. E.), the Leverhulme Trust (to G. G. T. and M. V.), the Royal Society (to M. V. and C. E. M.), the Wellcome Trust and the Leverhulme Trust (to C. M. D.) and the Australian Research Council (to J. A. C.).

‡ http://www-vendruscolo.ch.cam.ac.uk/zyggregator.php

References

1. Dobson, C. M. (2003). Protein folding and misfolding. *Nature*, **426**, 884–890.
2. Raso, S. W. & King, J. (2000). Protein folding and human disease. *Mechanisms of Protein Folding* (Pain, R. H., ed), 2nd edit., pp. 406–428, Oxford University Press, Oxford.
3. Selkoe, D. J. (2003). Folding proteins in fatal ways. *Nature*, **426**, 900–904.
4. Knowles, T. P., Smith, J. F., Craig, A., Dobson, C. M. & Welland, M. E. (2006). Spatial persistence of angular correlations in amyloid fibrils. *Phys. Rev. Letters*, **96**, 238–301.
5. Waterhouse, S. H. & Gerrard, J. A. (2004). Amyloid fibrils in bionanotechnology. *Aust. J. Chem.* **57**, 519–523.
6. Sunde, M. & Blake, C. (1997). The structure of amyloid fibrils by electron microscopy and X-ray diffraction. *Adv. Protein Chem.* **50**, 123–159.
7. Sunde, M., Serpell, L. C., Bartlam, M., Fraser, P. E., Pepys, M. B. & Blake, C. C. (1997). Common core structure of amyloid fibrils by synchrotron X-ray diffraction. *J. Mol. Biol.* **273**, 729–739.
8. Khurana, R., Ionescu-Zanetti, C., Pope, M., Li, J., Nielson, L., Ramirez-Alvarado, M. *et al.* (2003). A general model for amyloid fibril assembly based on morphological studies using atomic force microscopy. *Biophys. J.* **85**, 1135–1144.
9. Anderson, M., Bocharova, O. V., Makarava, N., Breydo, L., Salnikov, V. V. & Baskakov, I. V. (2006). Polymorphism and ultrastructural organization of prion protein amyloid fibrils: an insight from high resolution atomic force microscopy. *J. Mol. Biol.* **358**, 580–596.
10. Arimon, M., Diez-Perez, I., Kogan, M. J., Durany, N., Giralt, E., Sanz, F. & Fernandez-Busquets, X. (2005). Fine structure study of Aβ1-42 fibrillogenesis with atomic force microscopy. *FASEB J.* **19**, 1344–1346.
11. Sandilands, A., Hutcheson, A. M., Long, H. A., Prescott, A. R., Vrensen, G., Loster, J. *et al.* (2002). Altered aggregation properties of mutant γ-crystallins cause inherited cataract. *EMBO J.* **21**, 6005–6014.
12. Meehan, S., Berry, Y., Luisi, B., Dobson, C. M., Carver, J. A. & MacPhee, C. E. (2004). Amyloid fibril formation by lens crystallin proteins and its implications for cataract formation. *J. Biol. Chem.* **279**, 3413–3419.
13. Kosinski-Collins, M. S. & King, J. (2003). *In vitro* unfolding, refolding, and polymerization of human γD crystallin, a protein involved in cataract formation. *Protein Sci.* **12**, 480–490.
14. Wistow, G. J. & Piatigorsky, J. (1988). Lens crystallins: the evolution and expression of proteins for a highly specialized tissue. *Annu. Rev. Biochem.* **57**, 479–504.
15. Goldstein, L. E., Muffat, J. A., Cherny, R. A., Moir, R. D., Ericsson, M. H., Huang, X. *et al.* (2003). Cytosolic β-amyloid deposition and supranuclear cataracts in lenses from people with Alzheimer's disease. *Lancet*, **361**, 1258–1265.
16. Horwitz, J. (2003). α-Crystallin. *Exp. Eye Res.* **76**, 145–153.
17. Derham, B. K. & Harding, J. J. (1999). α-Crystallin as a molecular chaperone. *Prog. Retin. Eye Res.* **18**, 463–509.
18. Sun, Y. & MacRae, T. H. (2005). The small heat shock proteins and their role in human disease. *FEBS J.* **272**, 2613–2627.
19. Perng, M. D., Muchowski, P. J., van Den, I. P., Wu, G. J., Hutcheson, A. M., Clark, J. I. & Quinlan, R. A. (1999). The cardiomyopathy and lens cataract mutation in αB-crystallin alters its protein structure, chaperone activity, and interaction with intermediate filaments *in vitro*. *J. Biol. Chem.* **274**, 33235–33243.
20. Perng, M. D., Wen, S. F., van den, I. P., Prescott, A. R. & Quinlan, R. A. (2004). Desmin aggregate formation by R120G αB-crystallin is caused by altered filament interactions and is dependent upon network status in cells. *Mol. Biol. Cell*, **15**, 2335–2346.
21. Vicart, P., Caron, A., Guicheney, P., Li, Z., Prevost, M. C., Faure, A. *et al.* (1998). A missense mutation in the αB-crystallin chaperone gene causes a desmin-related myopathy. *Nature Genet.* **20**, 92–95.
22. Sanbe, A., Osinska, H., Villa, C., Gulick, J., Klevitsky, R., Glabe, C. G. *et al.* (2005). Reversal of amyloid-induced heart disease in desmin-related cardiomyopathy. *Proc. Natl Acad. Sci. USA*, **102**, 13592–13597.
23. Sanbe, A., Yamauchi, J., Miyamoto, Y., Fujiwara, Y., Murabe, M. & Tanoue, A. (2007). Interruption of CryAB-amyloid oligomer formation by HSP22. *J. Biol. Chem.* **282**, 555–563.
24. de Jong, W. W., Leunissen, J. A. & Voorter, C. E. (1993). Evolution of the α-crystallin/small heat-shock protein family. *Mol. Biol. Evol.* **10**, 103–126.
25. van Montfort, R. L., Basha, E., Friedrich, K. L., Slingsby, C. & Vierling, E. (2001). Crystal structure and assembly of a eukaryotic small heat shock protein. *Nature Struct. Biol.* **8**, 1025–1030.
26. Kim, K. K., Kim, R. & Kim, S. H. (1998). Crystal structure of a small heat-shock protein. *Nature*, **394**, 595–599.
27. Aquilina, J. A., Benesch, J. L., Bateman, O. A., Slingsby, C. & Robinson, C. V. (2003). Polydispersity of a mammalian chaperone: mass spectrometry reveals the population of oligomers in αB-crystallin. *Proc. Natl Acad. Sci. USA*, **100**, 10611–10616.
28. Carver, J. A., Aquilina, J. A., Truscott, R. J. & Ralston, G. B. (1992). Identification by ^{1}H NMR spectroscopy of flexible C-terminal extensions in bovine lens α-crystallin. *FEBS Letters*, **311**, 143–149.
29. Sun, Y. & MacRae, T. H. (2005). Small heat shock proteins: molecular structure and chaperone function. *Cell Mol. Life Sci.* **62**, 2460–2476.
30. Haley, D. A., Horwitz, J. & Stewart, P. L. (1998). The small heat-shock protein, αB-crystallin, has a variable quaternary structure. *J. Mol. Biol.* **277**, 27–35.
31. Glenner, G. G., Eanes, E. D. & Page, D. L. (1972). The relation of the properties of Congo red-stained amyloid fibrils to the β-conformation. *J. Histochem. Cytochem.* **20**, 821–826.
32. LeVine, H., 3rd (1999). Quantification of β-sheet amyloid fibril structures with thioflavin T. *Methods Enzymol.* **309**, 274–284.
33. Klunk, W. E., Pettegrew, J. W. & Abraham, D. J. (1989). Quantitative evaluation of congo red binding to amyloid-like proteins with a β-pleated sheet conformation. *J. Histochem. Cytochem.* **37**, 1273–1281.
34. Nilsson, M. R. (2004). Techniques to study amyloid fibril formation *in vitro*. *Methods*, **34**, 151–160.
35. Khurana, R., Coleman, C., Ionescu-Zanetti, C., Carter, S. A., Krishna, V., Grover, R. K. *et al.* (2005). Mechanism of thioflavin T binding to amyloid fibrils. *J. Struct. Biol.* **151**, 229–238.
36. Frederikse, P. H. (2000). Amyloid-like protein structure in mammalian ocular lenses. *Curr. Eye Res.* **20**, 462–468.
37. Nilsberth, C., Westlind-Danielsson, A., Eckman, C. B., Condron, M. M., Axelman, K., Forsell, C. *et al.* (2001). The 'Arctic' APP mutation (E693G) causes Alzheimer's disease by enhanced Aβ protofibril formation. *Nature Neurosci.* **4**, 887–893.
38. Bucciantini, M., Giannoni, E., Chiti, F., Baroni, F.,

Formigli, L., Zurdo, J. *et al.* (2002). Inherent toxicity of aggregates implies a common mechanism for protein misfolding diseases. *Nature*, **416**, 507–511.
39. Doss-Pepe, E. W., Carew, E. L. & Koretz, J. F. (1998). Studies of the denaturation patterns of bovine α-crystallin using an ionic denaturant, guanidine hydrochloride and a non-ionic denaturant, urea. *Exp. Eye Res.* **67**, 657–679.
40. Esposito, G., Viglino, P., Fogolari, F., Gaestel, M. & Carver, J. A. (1998). Selective NMR experiments on macromolecules: implementation and analysis of QUIET-NOESY. *J. Magn. Reson.* **132**, 204–213.
41. Christodoulou, J., Larsson, G., Fucini, P., Connell, S. R., Pertinhez, T. A., Hanson, C. L. *et al.* (2004). Heteronuclear NMR investigations of dynamic regions of intact *Escherichia coli* ribosomes. *Proc. Natl Acad. Sci. USA*, **101**, 10949–10954.
42. Siemer, A. B., Arnold, A. A., Ritter, C., Westfeld, T., Ernst, M., Riek, R. & Meier, B. H. (2006). Observation of highly flexible residues in amyloid fibrils of the HET-s prion. *J. Am. Chem. Soc.* **128**, 13224–13228.
43. Bova, M. P., Yaron, O., Huang, Q., Ding, L., Haley, D. A., Stewart, P. L. & Horwitz, J. (1999). Mutation R120G in αB-crystallin, which is linked to a desmin-related myopathy, results in an irregular structure and defective chaperone-like function. *Proc. Natl Acad. Sci. USA*, **96**, 6137–6142.
44. Kelly, J. W. (1998). The alternative conformations of amyloidogenic proteins and their multi-step assembly pathways. *Curr. Opin. Struct. Biol.* **8**, 101–106.
45. Uversky, V. N. & Fink, A. L. (2004). Conformational constraints for amyloid fibrillation: the importance of being unfolded. *Biochim. Biophys. Acta*, **1698**, 131–153.
46. Pawar, A. P., Dubay, K. F., Zurdo, J., Chiti, F., Vendruscolo, M. & Dobson, C. M. (2005). Prediction of "aggregation-prone" and "aggregation-susceptible" regions in proteins associated with neurodegenerative diseases. *J. Mol. Biol.* **350**, 379–392.
47. Devlin, G. L., Knowles, T. P., Squires, A., McCammon, M. G., Gras, S. L., Nilsson, M. R. *et al.* (2006). The component polypeptide chains of bovine insulin nucleate or inhibit aggregation of the parent protein in a conformation-dependent manner. *J. Mol. Biol.* **360**, 497–509.
48. Clark, J. I. & Muchowski, P. J. (2000). Small heat-shock proteins and their potential role in human disease. *Curr. Opin. Struct. Biol.* **10**, 52–59.
49. Stege, G. J., Renkawek, K., Overkamp, P. S., Verschuure, P., van Rijk, A. F., Reijnen-Aalbers, A. *et al.* (1999). The molecular chaperone αb-crystallin enhances amyloid β neurotoxicity. *Biochem. Biophys. Res. Commun.* **262**, 152–156.
50. Raman, B., Ban, T., Sakai, M., Pasta, S. Y., Ramakrishna, T., Naiki, H. *et al.* (2005). αB-crystallin, a small heat-shock protein, prevents the amyloid fibril growth of an amyloid β-peptide and β2-microglobulin. *Biochem. J.* **392**, 573–581.
51. Reddy, G. B., Kumar, P. A. & Kumar, M. S. (2006). Chaperone-like activity and hydrophobicity of α-crystallin. *IUBMB Life*, **58**, 632–641.
52. Tompa, P. & Csermely, P. (2004). The role of structural disorder in the function of RNA and protein chaperones. *FASEB J.* **18**, 1169–1175.
53. Frare, E., Mossuto, M. F., Polverino de Laureto, P., Dumoulin, M., Dobson, C. M. & Fontana, A. (2006). Identification of the core structure of lysozyme amyloid fibrils by proteolysis. *J. Mol. Biol.* **361**, 551–561.
54. Harper, J. D., Wong, S. S., Lieber, C. M. & Lansbury, P. T., Jr (1999). Assembly of Aβ amyloid protofibrils: an *in vitro* model for a possible early event in Alzheimer's disease. *Biochemistry*, **38**, 8972–8980.
55. Makarava, N., Bocharova, O. V., Salnikov, V. V., Breydo, L., Anderson, M. & Baskakov, I. V. (2006). Dichotomous *versus* palm-type mechanisms of lateral assembly of amyloid fibrils. *Protein Sci.* **15**, 1334–1341.
56. Smith, J. F., Knowles, T. P., Dobson, C. M., MacPhee, C. E. & Welland, M. E. (2006). Characterization of the nanoscale properties of individual amyloid fibrils. *Proc. Natl Acad. Sci. USA*, **103**, 15806–15811.
57. Hatters, D. M., MacRaild, C. A., Daniels, R., Gosal, W. S., Thomson, N. H., Jones, J. A. *et al.* (2003). The circularization of amyloid fibrils formed by apolipoprotein C-II. *Biophys. J.* **85**, 3979–3990.
58. Lashuel, H. A. & Lansbury, P. T. (2006). Are amyloid diseases caused by protein aggregates that mimic bacterial pore-forming toxins? *Quart. Rev. Biophys.* **39**, 167–201.
59. Lashuel, H. A., Hartley, D., Petre, B. M., Walz, T. & Lansbury, P. T., Jr (2002). Neurodegenerative disease: amyloid pores from pathogenic mutations. *Nature*, **418**, 291.
60. Chiti, F., Stefani, M., Taddei, N., Ramponi, G. & Dobson, C. M. (2003). Rationalization of the effects of mutations on peptide and protein aggregation rates. *Nature*, **424**, 805–808.
61. DuBay, K. F., Pawar, A. P., Chiti, F., Zurdo, J., Dobson, C. M. & Vendruscolo, M. (2004). Prediction of the absolute aggregation rates of amyloidogenic polypeptide chains. *J. Mol. Biol.* **341**, 1317–1326.
62. Andley, U. P., Mathur, S., Griest, T. A. & Petrash, J. M. (1996). Cloning, expression, and chaperone-like activity of human αA-crystallin. *J. Biol. Chem.* **271**, 31973–31980.
63. Horwitz, J., Huang, Q. L., Ding, L. & Bova, M. P. (1998). Lens α-crystallin: chaperone-like properties. *Methods Enzymol.* **290**, 365–383.
64. Treweek, T. M., Rekas, A., Lindner, R. A., Walker, M. J., Aquilina, J. A., Robinson, C. V. *et al.* (2005). R120G αB-crystallin promotes the unfolding of reduced α-lactalbumin and is inherently unstable. *FEBS J.* **272**, 711–724.
65. Burgio, M. R., Bennett, P. M. & Koretz, J. F. (2001). Heat-induced quaternary transitions in hetero- and homo-polymers of α-crystallin. *Mol. Vis.* **7**, 228–233.
66. Squires, A. M., Devlin, G. L., Gras, S. L., Tickler, A. K., MacPhee, C. E. & Dobson, C. M. (2006). X-ray scattering study of the effect of hydration on the cross-β structure of amyloid fibrils. *J. Am. Chem. Soc.* **128**, 11738–11739.
67. Liu, M., Mao, X. A., Ye, C., Huang, H., Nicholson, J. K. & Lindon, J. C. (1998). Improved WATERGATE pulse sequences for solvent suppression in NMR spectroscopy. *J. Magn. Reson.* **132**, 125–129.
68. Dehner, A. & Kessler, H. (2005). Diffusion NMR spectroscopy: folding and aggregation of domains in p53. *Chembiochem.* **6**, 1550–1565.

Edited by K. Kuwajima

(Received 9 February 2007; received in revised form 19 June 2007; accepted 24 June 2007)
Available online 29 June 2007